Role of Entropy in Protein Thermostability: Folding Kinetics of a Hyperthermophilic Cold Shock Protein at High Temperatures Using ^{19}F NMR†

Benjamin Schuler,*,‡,§ Werner Kremer,§ Hans Robert Kalbitzer,§ and Rainer Jaenicke§

Institut für Biophysik und Physikalische Biochemie, Universität Regensburg, Universitätsstrasse 31, 93040 Regensburg, Germany, and Laboratory of Chemical Physics, National Institute of Diabetes and Digestive and Kidney Diseases, National Institutes of Health, Bethesda, Maryland 20892-0520

Received June 13, 2002; Revised Manuscript Received July 16, 2002

ABSTRACT: We used ^{19}F NMR to extend the temperature range accessible to detailed kinetic and equilibrium studies of a hyperthermophilic protein. Employing an optimized incorporation strategy, the small cold shock protein from the bacterium *Thermotoga maritima* (*Tm*Csp) was labeled with 5-fluorotryptophan. Although chaotropically induced unfolding transitions revealed a significant decrease in the stabilization free energy upon fluorine labeling, the protein's kinetic folding mechanism is conserved. Temperature- and guanidinium chloride-dependent equilibrium unfolding transitions monitored by ^{19}F NMR agree well with the results from optical spectroscopy, and provide a stringent test of the two-state folding character of *Tm*Csp. Folding and unfolding rate constants at high temperatures were determined from the ^{19}F NMR spectra close to the midpoint of thermal unfolding by global line shape analysis. In combination with results from stopped-flow experiments at lower temperatures, they show that the folding rate constant of *Tm*Csp and its temperature dependence closely resemble those of its mesophilic homologue from *Bacillus subtilis*, *Bs*CspB. However, the *un*folding rate constant of *Tm*Csp is two orders of magnitude lower over the entire temperature range that was investigated. Consequently, the difference in conformational stability between the two proteins is solely due to the unfolding rate constant over a wide temperature range. A thermodynamic analysis points to an important role of entropic factors in the stabilization of *Tm*Csp relative to its mesophilic homologues.

Proteins from thermophilic organisms exhibit remarkable thermal stability, making life possible at temperatures above the boiling point of water. Despite two decades of active research in this field, a general concept of how this stability is achieved has remained elusive (*1*). The small differences that are necessary in terms of stabilization free energy appear to be implemented by a variety of strategies using combinations of virtually all known structural parameters (*2*, *3*). Experimental analyses of the kinetic and thermodynamic basis of thermostability, which might extend our understanding beyond the static picture from sequence and structure comparisons, have often been hampered by the irreversible unfolding of thermophilic proteins (*4*). Recently, protein families have been identified that do not show these complications and allow a comparison of homologous proteins from organisms with different thermophilicities (*5*−*7*). To extend the temperature range and detail accessible to the investigation of the folding of the cold shock protein from the hyperthermophilic bacterium *Thermotoga maritima* (*Tm*Csp,[1] Figure 1) (*5*, *8*, *9*), we decided to use NMR. This method allows not only simultaneous monitoring of multiple nuclei in a protein individually but also the extraction of kinetic parameters from equilibrium measurements by line shape analysis (*10*). Due to signal overlap in proton NMR spectra, detailed analyses of this kind have so far been limited to the signals from aromatic amino acids in very small proteins (*10*−*15*). With its large fraction of aromatic amino acids, the assignment and separation of single resonances were not possible in proton spectra of *Tm*Csp, particularly in the unfolding transition region. Thus, selective labeling of specific atoms or amino acid side chains had to be applied. Here we use ^{19}F as a nucleus, which combines several advantages, including 100% natural abundance, a receptivity to NMR detection close to that of the proton, a large chemical shift range, and exquisite sensitivity for changes in the local van der Waals environment and electrostatic fields (*16*−*19*).

Most commonly, aromatic amino acids labeled with ^{19}F at one of the ring positions are incorporated biosynthetically by microbial protein expression in the presence of the desired amino acid analogue. The ability of cells to synthesize that

† This work was supported by the Fonds der Chemischen Industrie and the Deutsche Forschungsgemeinschaft. B.S. was supported by an Emmy Noether-Fellowship from the Deutsche Forschungsgemeinschaft.

* To whom correspondence should be addressed: Laboratory of Chemical Physics, National Institute of Diabetes and Digestive and Kidney Diseases, National Institutes of Health, Bethesda, MD 20892-0520. Phone: (301) 402-1198. Fax: (301) 496-0825. E-mail: schuler@helix.nih.gov. Current address: Physikalische Biochemie, Universität Potsdam, 14476 Golm, Germany. Phone: +49 (331) 977 5244. Fax: +49 (331) 977 5062. E-mail: bschuler@rz.uni-potsdam.de.

‡ National Institutes of Health.

§ Universität Regensburg.

[1] Abbreviations: *Tm*Csp, cold shock protein from *T. maritima*; *Bs*CspB, cold shock protein from *Bacillus subtilis*; *Bc*Csp, cold shock protein from *Bacillus caldolyticus*; CD, circular dichroism; DSC, differential scanning calorimetry; OD_{555}, optical density at 555 nm; IPTG, isopropyl β-D-thiogalactoside; GdmCl, guanidinium chloride; 5-F-Trp, 5-fluorotryptophan; *Tm*CspFW, *Tm*Csp labeled with 5-F-Trp; DSS, dimethylsilapentanesulfonic acid.

10.1021/bi026293l CCC: $22.00
Published on Web 08/17/2002

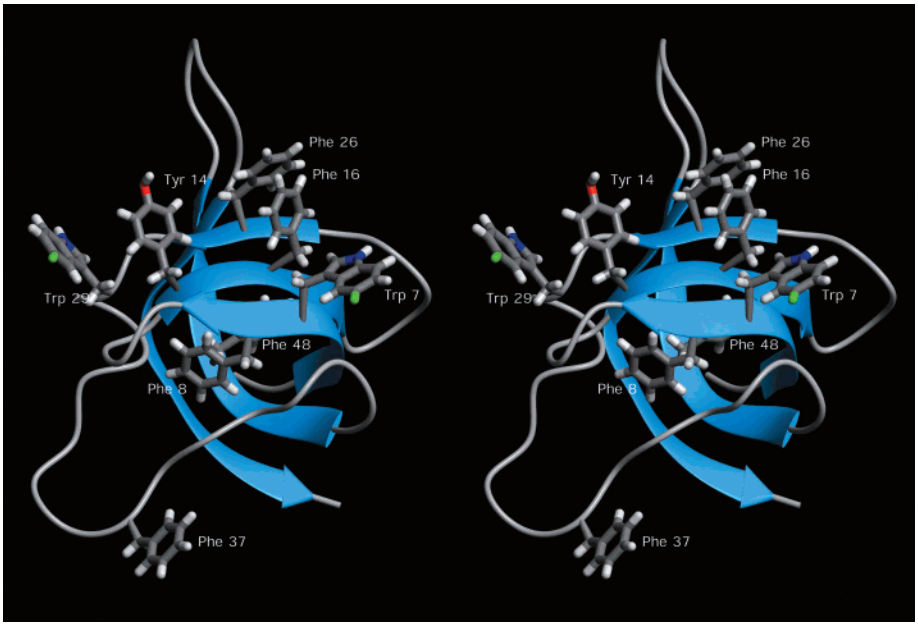

FIGURE 1: Stereo ribbon drawing of the tertiary structure of Csp from *T. maritima*. The aromatic side chains, which form a hydrophobic cluster on the surface, are shown in a cone representation. The positions of fluorine in the protein labeled with 5-F-Trp are colored in green. This figure was prepared using Molmol (*54*).

amino acid endogenously is most easily eliminated by adding the herbicide glyphosate, which inhibits the de novo synthesis of the aromatic amino acids (*20*, *21*). However, this strategy is often hampered by incomplete incorporation (*20*), which introduces heterogeneity into the sample and can even obscure its folding behavior, if species with different degrees of labeling have different conformational stabilities or folding kinetics. Here, we describe a modified growth protocol, which permits complete incorporation of [^{19}F]Trp. We used the altered absorbance of the fluorinated tryptophan side chains to conveniently determine the level of incorporation spectroscopically. Monitoring GdmCl- and temperature-induced equilibrium unfolding transitions by one-dimensional (1D) ^{19}F NMR spectra allowed us to stringently test the two-state folding behavior of *Tm*Csp and measure folding and unfolding rate constants at high temperatures by complete line shape analysis. Being able to measure both thermodynamic and kinetic parameters over a wide temperature range allows a much more detailed analysis of the kinetic and thermodynamic mechanism of thermostability of this protein than previously possible. The increased thermostability of *Tm*Csp compared to that of the highly homologous CspB from *Bacillus subtilis* (*22*) is found to be due to lower unfolding rate constants over a wide temperature range, whereas the folding rate constants and their temperature dependences are very similar for the two proteins. This leads us to conclude that entropic factors play an important role in the thermostabilization of *Tm*Csp.

MATERIALS AND METHODS

Ultrapure GdmCl was from ICN (Cleveland, OH). All other chemicals were obtained from Sigma-Aldrich or Merck at analytical grade. The herbicide Roundup (Monsanto) was used as a cost-saving source of glyphosate. Chromatography material was from Pharmacia-Amersham, and YM3 ultrafiltration membranes from Amicon were used for the concentration of protein solutions. Refractive index measurements were used to determine GdmCl concentrations (*23*). Protein concentrations were determined by absorbance spectroscopy (*24*, *25*) using a molar extinction coefficient of 1.28×10^3 M^{-1} cm^{-1} for unlabeled *Tm*Csp (*8*) and molar extinction coefficients for labeled *Tm*Csp as described below. All measurements were performed in buffer containing 50 mM sodium phosphate, 20 mM NaCl, 0.2 mM EDTA, and 1 mM DTE (pH 6.5) unless stated otherwise. SigmaPlot (Jandel) was used for regression analysis.

Mutagenesis, Incorporation of Fluorine, and Protein Purification. One of the major problems with the incorporation of some of the fluorinated amino acids into proteins is their toxicity to bacterial cells (*21*). Inclusion of ~10−20% of the unlabeled analogue in the growth medium has been suggested (*20*), which increases the viability of the cells. However, if the labeling changes the stability or folding mechanism of the protein, the resulting incomplete incorporation of the fluorine label leads to a heterogeneous sample, which is prohibitive for an analysis of protein folding. Therefore, we grew bacterial cells in the presence of glyphosate with a limiting concentration of unlabeled Trp in the medium to allow for the buildup of a biosynthetic machinery unaffected by the toxic effects of the fluorine-labeled amino acid. When the cell culture started to reach the stationary phase due to a limiting Trp concentration, 5-F-Trp was added and protein expression was induced. If a sufficiently tightly regulated expression system is used, this procedure ensures high viability of the cells and complete incorporation of the respective amino acid.

The cold shock protein from *T. maritima* (*Tm*Csp) was expressed in *Escherichia coli* BL21(DE3) using a pET21a vector as described previously (*8*). Single tryptophan mutants were cloned using the Stratagene Quickchange site-directed mutagenesis kit and the primers 5′-CATATGAGAGGAAAGGTTAAGTACTTCGATTCCAAGAAGGGCTACGG-3′ and 5′-CCGTAGCCCTTCTTGGAATCGAAGTACTTAACCTTTCCTCTCATATG-3′ to substitute a tyrosine residue for

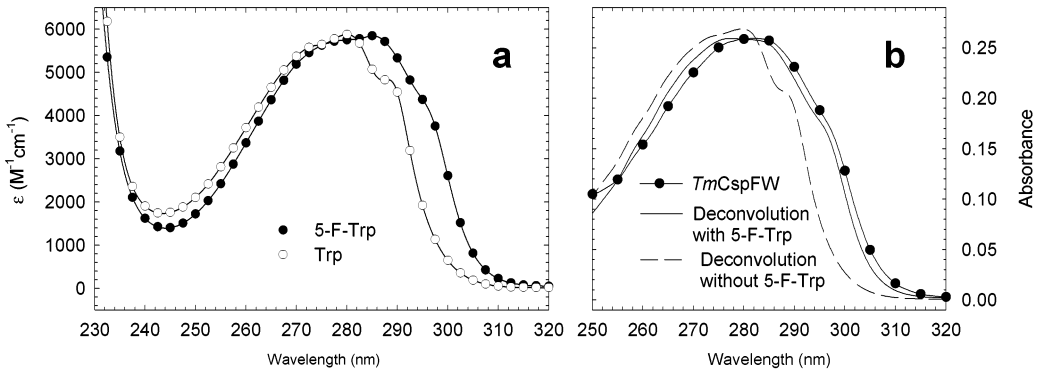

FIGURE 2: Absorbance of 5-F-Trp in comparison to that of unlabeled Trp and deconvolution of fluorine-labeled *Tm*Csp using the absorbance spectra of isolated aromatic amino acids in 6 M GdmCl. (a) Absorbance spectra of Trp and 5-F-Trp in 6 M GdmCl showing the strong bathochromic effect caused by the fluorine atom. (b) The absorbance spectrum of *Tm*Csp labeled with 5-F-Trp (*Tm*CspFW), denatured in 6 M GdmCl (●), can be well deconvolved using a sum of the absorbance spectra of Phe, Tyr, and 5-F-Trp (solid line). The optimum deconvolution using the spectra of Phe, Tyr, and unlabeled Trp is shown as a dashed line.

Table 1: Extinction Coefficients[a] of 5-F-Trp

	262 nm	271 nm	280 nm	290 nm	300 nm
water	$(4.0 \pm 0.2) \times 10^3$	$(5.4 \pm 0.2) \times 10^3$	$(5.7 \pm 0.3) \times 10^3$	$(5.1 \pm 0.2) \times 10^3$	$(2.05 \pm 0.09) \times 10^3$
6 M GdmCl	$(3.76 \pm 0.05) \times 10^3$	$(5.31 \pm 0.06) \times 10^3$	$(5.75 \pm 0.07) \times 10^3$	$(5.33 \pm 0.06) \times 10^3$	$(2.61 \pm 0.03) \times 10^3$

[a] Extinction coefficients are given in M^{-1} cm^{-1}.

Trp7 and introduce a diagnostic *Sca*I restriction site (mutant W7Y) and the primers 5′-GGAGACGTGTTCGTACAC-TACTCAGCAATTGAAATGGAAGGTTTCAAAAC-3′ and 5′-GTTTTGAAACCTTCCATTTCAATTGCTGAGTAGTG-TACGAACACGTCTCC-3′ to replace Trp29 with tyrosine and introduce a diagnostic *Mun*I restriction site (mutant W29Y).

The unlabeled protein was expressed as described previously (*8*). For the introduction of fluorotryptophan, new minimal medium (NMM) was used (*26*) with all amino acids except for Trp at a final concentration of 50 mg/L. Trp was added to a final concentration of only 5 mg/L. All bacterial growth was under the selective pressure of 50 mg/L carbenicillin, and endogenous synthesis of aromatic amino acids was suppressed by glyphosate [*N*-(phosphonomethyl)-glycine] at a final concentration of 1 g/L. Medium was inoculated with a freshly transformed single colony of bacterial cells and shaken vigorously at 37 °C. Growth was monitored using the apparent optical density at a wavelength of 555 nm (OD_{555}). As soon as the culture left the exponential growth phase due to the limiting concentration of Phe or Trp (usually at an OD_{555} of ∼1.5), D/L-5-F-Trp was added to a final concentration of 50 mg/L, and protein expression was induced by the addition of 1 mM IPTG. Approximately 4 h after induction and further incubation at 37 °C, the cells were harvested, and *Tm*Csp was purified as described previously (*8*).

Optical Spectroscopy. Baseline-corrected absorbance spectra were recorded in a Jasco V-530 spectrometer. Deconvolution of absorbance spectra was carried out with the program SigmaPlot (Jandel). Fluorescence spectra were recorded using a Spex Fluoromax spectrofluorimeter. Circular dichroism spectra and temperature transitions were measured in an AVIV 62A-DS spectropolarimeter equipped with thermostated cell holder using calibrated fused silica cells (path length of 1.0 mm) at a protein concentration of 1 mg/mL.

Quantification of Fluorine Incorporation by Absorbance Spectroscopy. The substitution of a fluorine atom for a hydrogen atom bonded to the ring system of Trp changes the electronic properties of the chromophore and thus its electronic excitation and emission spectra (*27*). We used the absorbance spectrum of the individual amino acids Tyr, Trp, 5-F-Trp, and Phe in 6 M GdmCl to deconvolve the spectra of the labeled protein variants denatured in 6 M GdmCl to quantify the incorporation yield of labeling with 5-F-Trp. Figure 2a shows the absorbance spectrum of 5-F-Trp in direct comparison to that of Trp. The absorbance spectrum of the resulting labeled protein is changed accordingly (Figure 2b). Solutions with a known concentration of 5-F-Trp were prepared by weighing out the dry substance in triplicate and dissolving it in water or an aqueous 6 M GdmCl solution at neutral pH. The concentration of GdmCl did not affect the absorbance spectra of the isolated aromatic amino acids significantly. The extinction coefficients determined for 5-F-Trp at several wavelengths are given in Table 1. They can be used to determine the extinction coefficients of proteins containing 5-F-Trp in a manner analogous to established methods for the naturally occurring amino acids (*24*, *25*, *28*) according to the equation

$$\epsilon_{\text{native}} = \epsilon_{\text{denatured}}^{\text{GdmCl}} \frac{A_{\text{native}}}{A_{\text{denatured}}^{\text{GdmCl}}}$$

where ϵ_{native} is the extinction coefficient of the native protein and $\epsilon_{\text{denatured}}^{\text{GdmCl}}$ is the extinction coefficient of the denatured protein calculated from the sum of the contributing amino acids in 6 M GdmCl at the respective wavelength. A_{native} and $A_{\text{denatured}}^{\text{GdmCl}}$ are the absorbances of the native and denatured protein measured with protein solutions diluted from the same stock solution to identical final protein concentrations into buffer and GdmCl solutions, respectively.

The absorbance spectrum of *Tm*CspFW was analyzed assuming that only Phe, Tyr, Trp, and 5-F-Trp contribute significantly to the absorbance at wavelengths between 250 and 320 nm, and using the total number of Phe, Tyr, and

Table 2: ^{19}F NMR Parameters of 5-Fluorotryptophan in *Tm*CspFW

residue	native state[a] (300 K) δ (ppm)	thermally denatured (392 K) δ (ppm)	denatured in 6 M GdmCl (300 K) δ (ppm)	free 5-F-Trp (300 K) δ (ppm)
Trp7	−44.2	−47.2	−46.8	−47.0
Trp29	−47.6	−47.3	−46.8	

[a] All spectra were measured in 50 mM sodium phosphate, 20 mM NaCl, 0.2 mM EDTA, and 1 mM DTE (pH 6.5).

Trp residues present in the polypeptide as a constraint. The experimental data can be described well as a sum of these amino acid spectra, in contrast to the best fit composite spectrum assuming only incorporation of unmodified aromatic side chains (Figure 2b). The optimum fit was obtained by assuming the complete absence of unlabeled Trp. This result was confirmed by quantitative NMR. As expected, two resonances of equal intensity at −44.2 and −47.6 ppm were observed in the ^{19}F NMR spectra of *Tm*CspFW (Figures 5 and 6 and Table 2), compared to a resonance at −47.0 ppm for pure 5-F-Trp (Table 2). Integration of these lines and comparison with the ^{19}F NMR spectra of free 5-F-Trp at a known concentration under identical conditions gave an incorporation yield of 99 ± 3%. We also analyzed the samples with electron spray ionization mass spectrometry (ESI-MS). The upper bound for the unlabeled protein resulting from these measurements was ∼0.5%, and that for the singly labeled protein was ∼2%, corroborating virtually complete incorporation. Our analysis resulted in extinction coefficients of 1.30×10^4 M^{-1} cm^{-1} for *Tm*CspFW at 280 nm, using the values for unlabeled amino acids given by Pace et al. (*25*).

GdmCl-Induced Unfolding Transitions. Samples (1.5 μM protein) were incubated for ∼1 h at 298 K in buffer containing 50 mM sodium phosphate, 20 mM NaCl, 0.2 mM EDTA, 1 mM DTE (pH 6.5), and 8% D_2O in the presence of varying concentrations of GdmCl. Fluorescence was then measured at 337 nm (4 nm bandwidth) upon excitation at 280 nm for *Tm*Csp and 286 nm for *Tm*CspFW (3 nm bandwidth). Nonlinear regression was carried out assuming a two-state reaction between the folded and unfolded state and a linear dependence of the fluorescence emission of the folded and unfolded state on GdmCl concentration (*29*).

Folding kinetics were measured in a DX.17MV sequential mixing stopped-flow spectrometer from Applied Photophysics (Leatherhead, U.K.) by following the change in fluorescence above 300 nm upon excitation at 280 nm (10 nm bandwidth). To initiate unfolding, 15 μM native protein in buffer was diluted 11-fold with GdmCl solutions of varying concentrations to give the desired final GdmCl concentrations. To initiate refolding, 15 μM protein unfolded in 6 M GdmCl was diluted 11-fold with aqueous buffer or GdmCl solutions of varying concentrations to give the desired final GdmCl concentrations. Five to fifteen kinetic traces were averaged and analyzed as single-exponential functions. The GdmCl dependence of folding kinetics was fit using the equation

$$\lambda = k_{f,0} e^{m_f c_D} + k_{u,0} e^{m_u c_D}$$

where λ is the measured rate constant, $k_{f,0}$ and $k_{u,0}$ are the folding and unfolding rate constants, respectively, at a denaturant concentration of 0 M, and c_D is the denaturant concentration

$$m_f = \frac{\partial \ln k_f}{\partial c_D}$$

and

$$m_u = \frac{\partial \ln k_u}{\partial c_D}$$

For a protein folding according to a two-state reaction

$$D \underset{k_u}{\overset{k_f}{\rightleftharpoons}} N$$

this results in a linear dependence of folding and unfolding rate constants on denaturant concentration if λ is plotted on a logarithmic scale.

Differential Scanning Calorimetry. Samples at a protein concentration of 1 mg/mL were dialyzed against buffer containing 50 mM sodium phosphate, 20 mM NaCl, 0.2 mM EDTA, and 1 mM DTE (pH 6.5) for at least 12 h; then D_2O was added to a final concentration of 8%, and the sample and some reference dialysis buffer were filtered and degassed. Measurements were performed in a CSC 6100 II calorimeter (Calorimetry Sciences Corp., Provo, UT) at a scan rate of 1 K/min. Independent samples were tested for reversibility of the unfolding transition by repeated scanning. Data were analyzed using the deconvolution software CpCalc supplied by CSC. The partial specific volume of the protein was calculated from its amino acid composition to be 0.744 cm^3/g, and the exact concentration was determined by absorbance.

NMR Spectroscopy. All samples were dialyzed against buffer containing 50 mM sodium phosphate, 20 mM NaCl, 0.2 mM EDTA, and 1 mM DTE (pH 6.5), and then NaN_3, DSS, and D_2O were added to final concentrations of 5 mM, 0.1 mM, and 8%, respectively. A sample volume of 500 μL was used, and sample tubes were sealed by melting for high-temperature experiments. ^{19}F NMR spectra were obtained at 470 MHz in a Bruker DMX 500 spectrometer using an appropriately tuned 5 mm hydrogen probe. Ninety-degree flip-angle pulses were found to be ∼11.5 μs at 300 K for all samples. For the quantitative measurements, a pulse angle of 90° and a repetition time of 1 s were used. Under these conditions, no saturation of ^{19}F signals was observed. No pH correction was made for the D_2O content; no proton decoupling was used, and spectra were processed with 1 Hz of line broadening, which does not affect line shape significantly at the line widths observed in our ^{19}F spectra. Indirect referencing via ^{1}H NMR spectra and DSS (2,2-dimethyl-2-silapentane-5-sulfonic acid) was used. For this purpose, ^{1}H spectra of the samples were measured at 500 MHz under identical conditions just before ^{19}F data acquisition, and the absolute ^{1}H frequency of the DSS signal was multiplied by a scaling factor of 0.940 866 982 to obtain the reference frequency of trifluoroacetic acid (TFA) for ^{19}F spectra (*30*). Temperature calibration was performed using the known temperature dependence of the difference of the two ethylene glycol ^{1}H NMR resonances (*31*). Integration

of NMR signals was performed using PeakFit (Jandel) and Excel (Microsoft).

Thermal unfolding of thermostable proteins can be problematic due to the irreversible degradative reactions taking place at high temperatures (*32*), which can only be neglected if incubation at these conditions is limited to a short period of time. Due to the low signal-to-noise ratio of NMR experiments and the broad lines of the ^{19}F-labeled protein, spectra in the transition region of thermal unfolding of *Tm*CspFW had to be acquired for at least 1 h. Thus, even the use of fresh samples for each temperature could not completely prevent the slow appearance of small amounts of chemically modified polypeptides during data acquisition. From experiments with samples incubated at high temperatures for up to 10 h, we estimate the error introduced into our data to be less than 10%.

Line Shape Analysis. Folding and unfolding rate constants in the transition region of thermal melts were estimated from the line broadening in ^{19}F NMR spectra by nonlinear regression, using the solution for the kinetic equations describing the exchange between two states and the Bloch equations describing the spin−spin relaxation of a nucleus (*10*, *33*). The frequency dependence of the ^{19}F NMR line spectrum $I(\nu)$ was simulated by

$$I(\nu) = -C_0 \frac{P\left[1 + \tau\left(\frac{p_D}{T_{2N}} + \frac{p_N}{T_{2D}}\right)\right] + QR}{P^2 + R^2} \quad (1a)$$

where C_0 is a scaling factor that is proportional to the protein concentration, T_{2N} and T_{2D} are the apparent transverse relaxation times in the absence of exchange broadening of states N and D, respectively, which were determined by linear extrapolation of the pre- and posttransition baseline values into the transition region, and p_N and p_D are the fractional populations of the native and denatured states, respectively. The terms P, Q, and R are given by

$$P = \tau\left[\frac{1}{T_{2N}T_{2D}} - 4\pi^2\Delta\nu^2 + \pi^2(\delta\nu)^2\right] + \frac{p_N}{T_{2N}} + \frac{p_D}{T_{2D}} \quad (1b)$$

$$Q = \tau[2\pi\Delta\nu - \pi\delta\nu(p_N - p_D)] \quad (1c)$$

$$R = 2\pi\Delta\nu\left[1 + \tau\left(\frac{1}{T_{2N}} + \frac{1}{T_{2D}}\right)\right] + \pi\delta\nu\tau\left(\frac{1}{T_{2N}} + \frac{1}{T_{2D}}\right) + \pi\delta\nu(p_N - p_D) \quad (1d)$$

with

$$\delta\nu = \nu_N - \nu_D \quad (1e)$$

and

$$\Delta\nu = \frac{\nu_N + \nu_D}{2} - \nu \quad (1f)$$

where ν_N and ν_D are the resonance frequencies of a nucleus in the native and denatured states, respectively, which were estimated by extrapolation of the pre- and posttransition baseline values into the transition region using a quadratic function. With the folding and unfolding rate constants k_f and k_u, respectively, the exchange correlation time τ is defined as

$$\tau = \frac{1}{k_u + k_f} \quad (1g)$$

The relative populations of states D and N follow as

$$p_N = k_f\tau \text{ and } p_D = k_u\tau \quad (1h)$$

A sum of two functions $I(\nu)$ was used for a global fit of the doubly labeled protein, using independent values for T_{2N}, T_{2D}, ν_N, and ν_D and identical values for p_N, p_D, k_f, k_u, and C_0. Standard deviations for the folding und unfolding rate constants were estimated from fits using independent values for k_f and k_u for the two lines in exchange. The indirect fluor−proton spin−spin couplings to the protons in positions 4 ($H^{\epsilon 3}$), 6 ($H^{\eta 2}$), and 7 ($H^{\zeta 2}$) in 5-fluorotryptophan ($F^{\zeta 3}$) are 9.9 ± 0.1 Hz for $^3J(F^{\zeta 3}H^{\epsilon 3})$ and $^3J(F^{\zeta 3}H^{\eta 2})$ and 4.68 ± 0.07 Hz for $^5J(F^{\zeta 3}H^{\zeta 2})$ (measured in aqueous solution at 293 K and pH 6.5). They are not resolved in the protein and were neglected in the simulations since the inhomogeneous line broadening caused by these couplings is small compared to the homogeneous line widths.

Analysis of the Temperature Dependence of Folding and Unfolding Rate Constants. Assuming that the transition state ensembles for folding and unfolding are energetically similar and that the reaction is microscopically reversible, we used transition state theory to analyze the folding kinetics of *Tm*CspFW (*34*, *35*). Transition state theory relates a reaction rate constant k_x to the Gibbs free energy of the transition state $\Delta G_x^{\ddagger}$ relative to the initial state:

$$k_x = \epsilon \frac{k_B T}{h} e^{\Delta G_x^{\ddagger}(T)/RT} \quad (2)$$

where ϵ is the transmission coefficient, k_B and h are the Boltzmann and Planck constants, respectively, R is the gas constant, and T is the absolute temperature. In analogy to the equilibrium Gibbs free energy ΔG, the temperature dependence of $\Delta G_x^{\ddagger}$ is given by

$$\Delta G_x^{\ddagger}(T) = \Delta H_x^{\ddagger}(T_0) - T\Delta S_x^{\ddagger}(T_0) + \Delta c_{p,x}^{\ddagger}\left[(T - T_0) - T\ln\frac{T}{T_0}\right] \quad (3)$$

where $\Delta H_x^{\ddagger}$ is the enthalpy of activation, $\Delta S_x^{\ddagger}$ is the entropy of activation, $\Delta c_{p,x}^{\ddagger}$ is the difference in heat capacity between the final and the initial state, which is assumed to be independent of temperature in this derivation, and T_0 is the reference temperature, 298 K in our case. For the folding and unfolding rate constants k_f and k_u, respectively, eqs 2 and 3 yield the Eyring equations

$$k_f = \epsilon\frac{k_B}{h} e^{[\Delta S_f^{\ddagger}(T_0)]/R} T e^{\{-\Delta H_f^{\ddagger}(T_0) - \Delta c_{p,f}^{\ddagger}[(T-T_0) - T\ln(T/T_0)]\}/RT} \quad (4a)$$

and

$$k_u = \epsilon\frac{k_B}{h} e^{\Delta S_u^{\ddagger}(T_0)/R} T e^{\{-\Delta H_u^{\ddagger}(T_0) - \Delta c_{p,u}^{\ddagger}[(T-T_0) - T\ln(T/T_0)]\}/RT} \quad (4b)$$

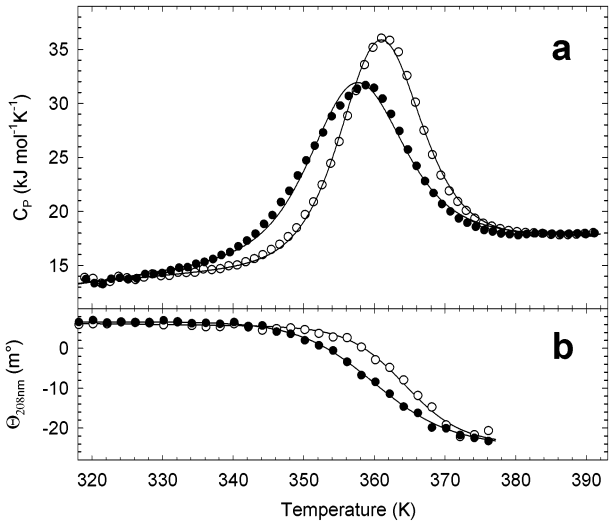

FIGURE 3: Thermal denaturation of fluorine-labeled (●, T_m = 359 K) and unlabeled (○, T_m = 361 K) *Tm*Csp. (a) Temperature dependence of the partial molar heat capacity measured by differential scanning calorimetry. Only every 12th data point is given. The solid lines show theoretical two-state approximations. (b) Temperature dependence of the circular dichroism signal at 208 nm for fluorine-labeled (●, T_m = 360 K) and unlabeled (○, T_m = 364 K) *Tm*Csp. Only every second data point is given. The solid lines show fits to a two-state model.

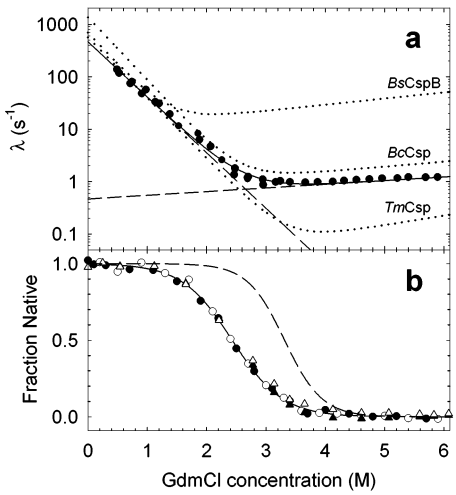

FIGURE 4: GdmCl dependence of the folding kinetics and equilibrium unfolding of labeled *Tm*Csp at 298 K. (a) Observed rate constant λ for folding and unfolding as a function of GdmCl concentration. A fit of the data to a two-state model (see Materials and Methods) is shown by the solid line. The dashed lines show the extrapolated GdmCl dependence of the microscopic folding and unfolding rate constants. The dotted lines represent the fits to corresponding data for the highly homologous unlabeled cold shock proteins from *B. subtilis* (*Bs*CspB), *B. caldolyticus* (*Bc*Csp), and *T. maritima* (*Tm*Csp) shown for comparison (parameters taken from ref *5*). (b) GdmCl-induced equilibrium unfolding transition measured by fluorescence [unfolding (●) and refolding (○)] and peak integration from 1D ^{19}F NMR spectra [signal from [^{19}F]Trp29 (△) and [^{19}F]Trp7 (▲)]. The fraction of native protein obtained from the fit to a two-state model is plotted, and the regression is indicated by the solid line. For comparison, the corresponding two-state fit for unlabeled *Tm*Csp is included (dashed line; parameters taken from ref *5*).

where $\Delta X^{\ddagger}_{f/u}$ values are the thermodynamic functions of the folding or unfolding reaction, i.e., the difference between X of the transition state and X of the unfolded or folded state, respectively. To be able to compare our data directly to those of Schindler and Schmid (*22*), we used a transmission coefficient of 1 in our analysis, which allows changes in activation entropies with temperature to be determined, although it clearly overestimates the absolute value of the preexponential factor (*36*) and does not take into account the temperature dependence of solvent viscosity.

RESULTS

Effects of Fluorine Labeling on Csp Structure and Thermostability. To be able to assess the validity of any conclusions drawn from folding analyses of *Tm*CspFW, in which both Trp residues of *Tm*Csp are replaced with 5-F-Trp, the structural integrity of the protein had to be verified. 1D ^{1}H NMR spectra exhibited the usual dispersion and peak distribution of native *Tm*Csp. Moreover, the similarity of far-UV CD spectra indicated virtually identical secondary structure content of labeled and unlabeled *Tm*Csp (data not shown), as expected for fluorine incorporation (*17*). Effects on thermostability were investigated by CD and differential scanning calorimetry (DSC). The melting temperature for *Tm*CspFW was 359 K, compared to 361 K for *Tm*Csp using DSC (Figure 3a). In spectropolarimetric measurements, 360 K was observed as the transition midpoint for *Tm*CspFW from the fit to a two-state model, compared to 364 K for the unlabeled protein (Figure 3b). Slight differences between the two methods are probably due to the high melting point of the protein and the resulting uncertainty of posttransition baselines in CD experiments (*8*). Temperature-induced unfolding was found to be reversible by repeated heating of the same samples to 375 K. A theoretical two-state approximation of the DSC data gave good fits (Figure 3a), and the ratio of calorimetric to van't Hoff unfolding enthalpies was close to unity for all samples as expected for a two-state transition (*37*), similar to what was found for the unlabeled protein (*38*). Despite slight effects on the melting temperature, fluorine labeling of *Tm*Csp therefore conserved both the thermostability and the two-state characteristics of the protein.

Effect of Fluorine Labeling on the Folding of TmCspFW in GdmCl. Unlike thermal unfolding transitions, GdmCl-induced unfolding transitions of *Tm*CspFW exhibited a clear shift of the midpoint, $c_{1/2}$, to lower GdmCl concentrations by ~1 M and a slight decrease in cooperativity, *m*, compared to that of unlabeled *Tm*Csp (Figure 4). This corresponds to a decrease in the Gibbs free energy of stabilization extrapolated to 0 M GdmCl, ΔG^0, by ~10 kJ/mol, to 14 ± 2 kJ/mol (*5*, *8*), a destabilization much greater than that typically reported for fluorine-labeled proteins (*17*−*19*). This decrease in stability also manifested itself in the dependence of the folding kinetics on GdmCl concentration (Figure 4a): the extrapolated folding rate constant in the absence of denaturant, k_f^0 = 470 s^{-1}, and its linear change with GdmCl concentration, m_f, were virtually identical to those of unlabeled *Tm*Csp, but the unfolding branch of the chevron plot was shifted to higher unfolding rate constants with a k_u^0 of 0.47 s^{-1} (Figure 4a). Both ΔG^0 and its GdmCl dependence calculated from kinetic and equilibrium data were in good agreement. Identical values were obtained for the apparent folding rate constant λ for unfolding and refolding experiments at the same concentration of denaturant, and the analysis of the amplitudes of the monophasic

unfolding and refolding kinetics of *Tm*CspFW (*39*) provided no evidence for rapidly formed folding intermediates (data not shown). Despite the significant effect of fluorine incorporation on its stability, these observations strongly support the assumption that the folding of *Tm*CspFW is a reversible two-state reaction, and that the folding mechanism of *Tm*Csp is conserved.

Investigation of Two-State Folding by ^{19}F NMR. To be able to assign the fluorine resonances of Trp7 and Trp29 in the native and denatured states of the protein, single-tryptophan mutants (W7Y and W29Y) were created by site-directed mutagenesis and labeled with 5-F-Trp. Under native conditions, the mutants exhibited ^{19}F NMR spectra with single peaks at −44.2 ppm for W29Y and −47.6 ppm for W7Y (data not shown), allowing unequivocal assignment of the resonances of the doubly labeled protein. Moreover, identical peak positions in *Tm*CspFW and the single-tryptophan mutants indicate a lack of direct interactions between the two tryptophan side chains, which makes them independent probes for monitoring the folding reaction and allows an even more stringent test of the two-state model than with optical methods. A GdmCl-induced unfolding transition of *Tm*CspFW monitored by ^{19}F NMR is shown in Figure 5. Above 1 M GdmCl, the intensity of the signals from W7 and W29 decreased synchronously with the simultaneous appearance of a single resonance for the denatured protein close to the signal of free 5-F-Trp (Table 2). This suggests the absence of secondary or tertiary structure in the unfolded state. There was hardly any dependence of the chemical shifts of all three peaks on GdmCl concentration, which means that there are no detectable changes in the electronic vicinity of the fluorine atoms, and therefore that the conformational ensembles of both the native and the denatured state do not undergo significant changes in protein structure or dynamics with changing GdmCl concentration. Calculating the fraction of native protein from the peak integrals yielded unfolding transitions that agree well with the transition obtained from fluorescence measurements (Figure 4b), which is compelling evidence for the good agreement of the equilibrium folding of *Tm*CspFW with a two-state model.

Temperature Dependence of Folding by ^{19}F NMR and Stopped Flow. The T_m of 356 K determined from the ^{19}F NMR spectra taken between 300 and 392 K (Figure 6) is close to the values obtained from CD and calorimetry (Figure 3), but several differences compared to the GdmCl-induced unfolding transition are obvious. First of all, there were both a pronounced temperature dependence of the chemical shifts and a gradual narrowing of the lines in the pretransition region. The increasing thermal motion in the native protein (*40*) can probably account for these effects without having to invoke major structural changes or folding pretransitions. Above 370 K, two sharp lines were observed in the denatured state (Figure 6) that were assigned from the single-tryptophan mutants under identical conditions (data not shown). The chemical shift difference between the lines was approximately constant over the entire posttransition region, indicating stable residual structure in the thermally unfolded state. No indication for secondary or tertiary structure was found in GdmCl-denatured *Tm*CspFW (see above, Figure 5). This discrepancy is in agreement with the dependence of residual structure on unfolding conditions in the denatured states of other proteins (*41*−*43*), and can probably be accounted for by the shielding of electrostatic interactions at high concentrations of GdmCl.

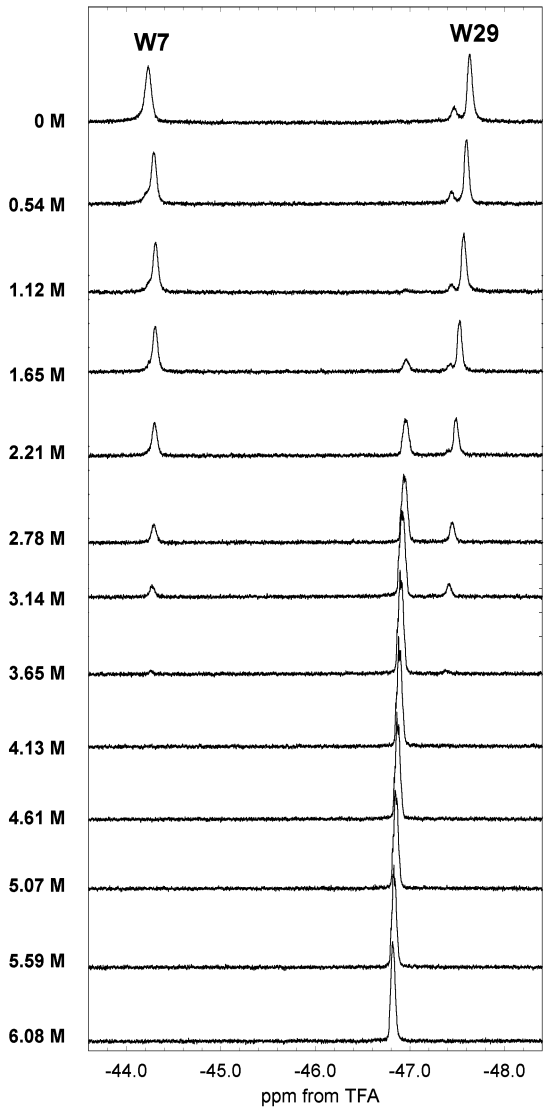

FIGURE 5: ^{19}F NMR spectra of 5-F-Trp-labeled *Tm*Csp as a function of GdmCl concentration measured at 298 K. Data were taken at a ^{19}F frequency of 470 MHz and indirectly referenced relative to TFA using ^{1}H spectra recorded under identical conditions. The vertical displacement of the spectra is proportional to the GdmCl concentration in the sample, which is indicated to the left of each spectrum. The resonances were assigned using site-directed mutagenesis.

Around the folding temperature, chemical exchange between folded and unfolded states leads to obvious line broadening, especially for the W7 resonance (Figure 6). This can be exploited to obtain folding and unfolding rate constants at high temperatures, using the functions describing NMR spectra of systems undergoing chemical exchange (*10*, *33*; see Materials and Methods). The method is limited to conditions significantly populating both the folded and the denatured state and yields greater uncertainty in the values determined than fluorescence stopped-flow techniques; however, it extends the measurable range of rate constants beyond that of conventional techniques (*10*−*12*, *15*), and it facilitates high-temperature measurements. Global line shape analysis of the spectra in the temperature range between 347 and 362 K assuming a two-state reaction yielded good fits (Figure

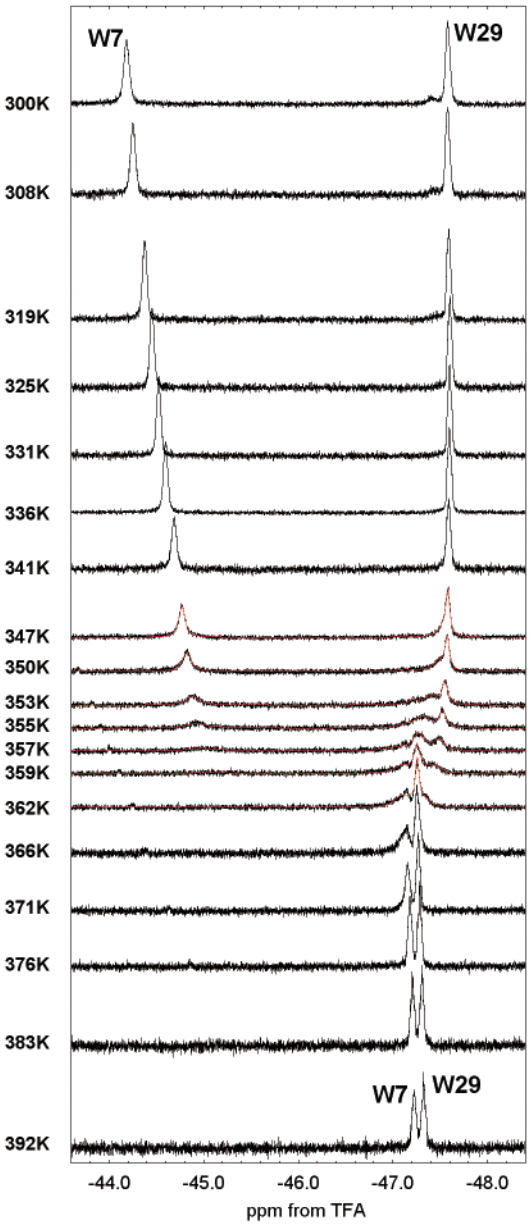

FIGURE 6: ^{19}F NMR spectra of 5-F-Trp-labeled *Tm*Csp as a function of temperature. Data were taken at a ^{19}F frequency of 470 MHz and indirectly referenced relative to TFA using ^{1}H spectra recorded under identical conditions. The vertical displacement of the spectra is proportional to temperature, which is indicated to the left of each spectrum. The resonances were assigned using site-directed mutagenesis. Line broadening in the transition region due to chemical exchange between native and denatured states can be utilized to determine folding and unfolding rate constants at these temperatures. Red lines show the corresponding fits from line shape analysis (see Materials and Methods).

6). Unfolding rate constants that increased from ~40 s^{-1} at 347 K to ~300 s^{-1} at 362 K were obtained, along with less temperature-dependent folding rate constants of ~200 s^{-1} (Figure 7).

Together with the values from the stopped-flow experiments between 290 and 318 K, the unfolding rate constant increased by 3 orders of magnitude over a temperature range of 72 K (Figure 7). The unfolding rate constant of *Tm*CspFW is almost independent of GdmCl concentration (Figure 4), which implies a transition state that is very nativelike in its interactions with the denaturant, a property that is closely

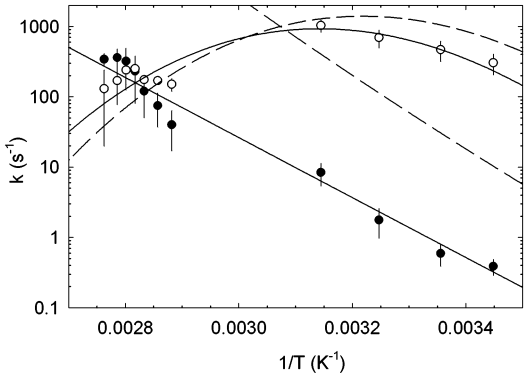

FIGURE 7: Analysis of the temperature dependence of the folding (○) and unfolding (●) rate constants of labeled *Tm*Csp. The values at low temperatures are from stopped-flow experiments, and the values at high temperatures are from dynamic NMR (Figure 6). The solid lines represent fits of the temperature dependence of the unfolding and folding rate constants according to transition state theory (eqs 4a and 4b). The temperature dependences of the folding and unfolding rate constants of *Bs*CspB (parameters taken from ref *22*) are shown as dashed lines for comparison.

Table 3: Comparison of Thermodynamic and Kinetic Parameters for *Tm*CspFW and *Bs*CspB at 298 K

	*Tm*Csp	*Bs*CspB[a]
$\Delta G°$ (equilibrium[b]) (kJ mol^{-1})	14 ± 2	8.9
m (equilibrium) (kJ mol^{-1} M^{-1})	−5.6 ± 0.2	
k_f^0 (s^{-1})	470	
k_u^0 (s^{-1})	0.47	
$\Delta G°$ (kinetic[c]) (kJ mol^{-1})	17 ± 2	
RTm_f (kJ mol^{-1} M^{-1})	−6.1 ± 0.2	
RTm_u (kJ mol^{-1} M^{-1})	0.40 ± 0.02	
$\Delta H_f^{\ddagger}$ (kJ mol^{-1})	51 ± 2	32 ± 2
$\Delta c_{p,f}^{\ddagger}$ (kJ mol^{-1} K^{-1})[d]	−2.6 ± 0.2	−2.7 ± 0.3
$\Delta H_u^{\ddagger}$ (kJ mol^{-1})	72 ± 2	96 ± 3
$\Delta c_{p,u}^{\ddagger}$ (kJ mol^{-1} K^{-1})[d]	0.2 ± 0.2	0.3 ± 0.4

[a] Data taken from ref *22*. [b] Obtained from GdmCl-induced equilibrium unfolding transitions (Figure 4b). [c] Obtained from the GdmCl dependence of the folding and unfolding kinetics (Figure 4a). [d] Assumed to be independent of temperature.

linked to the heat capacity change, because both values depend on the difference in solvent accessible surface area upon unfolding (*44*). Correspondingly, the curvature of the temperature dependence of the unfolding rate constant of *Tm*CspFW is also very small (Figure 7), yielding a $\Delta c_{p,u}^{\ddagger}$ close to zero (Table 3). The folding rate constant is much less temperature-dependent than the unfolding rate constant in the range investigated here. As the transition state and denatured state are very dissimilar in their interactions with the solvent (Figure 4; see above), the heat capacity difference between these two states is large. Using eq 4a, we obtained a value of −2.6 ± 0.2 kJ mol^{-1} K^{-1}, with an activation enthalpy for folding $\Delta H_f^{\ddagger}$ of 51 ± 2 kJ/mol at 298 K. Due to the large negative $\Delta c_{p,f}^{\ddagger}$, $\Delta H_f^{\ddagger}$ decreases with temperature. At low temperatures it is positive but becomes zero at ~318 K, and at higher temperatures, it is negative, implying that the barrier to refolding is of both enthalpic and entropic origin at low, but of entirely entropic origin at high, temperatures. This non-Arrhenius behavior of protein folding rates is well-established (*45*, *46*). A very similar temperature dependence was found for the folding kinetics of *Bs*CspB (*22*; Figure 7).

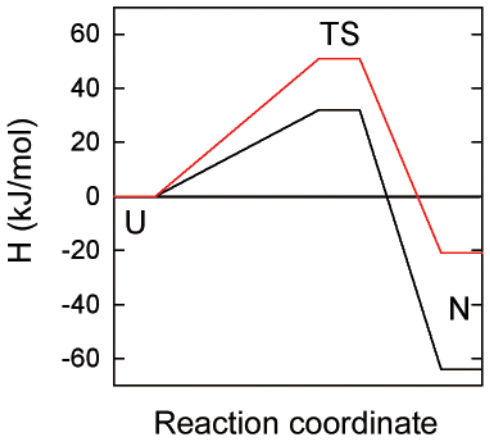

FIGURE 8: Schematic enthalpy diagram for *Bs*CspB (black) and labeled *Tm*Csp (red) at 298 K. The values for the native (N) and transition state (TS) are plotted relative to that of the denatured state (U).

As opposed to the strikingly similar *folding* rates of *Tm*CspFW and *Bs*CspB, the *unfolding* rate constants are almost 2 orders of magnitude higher for *Bs*CspB over the whole temperature range that was investigated (Figure 7). From the work of Perl et al. (*5*), it has been known that at 298 K, the differences in stability between *Bs*CspB, Csp from *Bacillus caldolyticus* (*Bc*Csp), and *Tm*Csp are entirely due to different unfolding rate constants, whereas the folding rate constants and the dependences of both folding and unfolding rate constants on GdmCl concentration are virtually identical for the three proteins. Our results suggest that the similarities in the folding kinetics and mechanism found for the mesophilic and hyperthermophilic cold shock proteins at ambient temperature extend to their temperature dependence: the lower unfolding rate constants of *Tm*Csp can also account for the different melting temperatures of *Bs*CspB and *Tm*Csp. In other words, the mechanism of stabilization of the thermophilic versus the mesophilic protein is conserved from room temperature to the physiological temperature of *Thermotoga* beyond 80 °C.

DISCUSSION

The conservation of the temperature dependences of folding and unfolding in this family of small cold shock proteins has implications for the structural interpretation of their different conformational stabilities. In this case, their different stabilities are completely due to different unfolding rate constants, but what is the origin of the large increase in the activation barrier for unfolding? One possible explanation would be a stabilization of the native state by means of surface mutations leading to a larger number of enthalpic interactions that form only after the transition state (*5*). Assuming that the energetics of the unfolded states of the three Csp variants are very similar, one would then expect increasing activation enthalpies of unfolding with increasing thermostability. However, as shown in Figure 8, the activation enthalpy of unfolding and even more the equilibrium unfolding enthalpy at 298 K are significantly *lower* for the thermophilic protein, which shows that enthalpic contributions can obviously not explain its increased stability. The activation enthalpy corresponds to the slope of the Arrhenius plot (the graph of ln k_u as a function of $1/T$, Figure 7), and to a first approximation, the activation entropy is proportional to the intercept with the ordinate. The large virtually parallel shift of the unfolding rate constants in Figure 7 therefore points to entropic factors dominating the effects of amino acid exchanges that lead to thermostability. Even if $\Delta c_{p,u}^{\ddagger}$ is varied between 0 and 400 J mol^{-1} K^{-1}, it is obvious from an analysis using eq 4b that the difference between the activation free energies of unfolding of *Tm*CspFW and *Bs*CspB is to a large part due to a difference in the activation *entropies* of unfolding.

Assigning these entropic factors to contributions from either solvent entropy or protein conformational entropy in experimental studies is complicated by the fact that solvent and protein form one thermodynamic system. Here, the only hint comes from the solvent dependence of the activation entropy. For *Bs*CspB, it was found that, compared with the *folding* activation entropy, the *unfolding* activation entropy hardly changed with urea concentration (*22*). This argues that most of the entropy difference between the transition state and the folded state is not due to different solvent interactions, but rather due to a reduction of the degrees of freedom accessible to the protein, e.g., by tighter core packing or reduced surface side chain flexibility. Therefore, it appears to be probable that changes in conformational entropy on the native side of the barrier can be modulated more easily than solvent entropy to achieve a decrease in free energy of the folded protein. This illustrates a situation where the mechanism of thermostabilization is inaccessible to approaches using the comparison of static structures, one of the classical strategies in the field (*2*), but rather requires kinetic and thermodynamic or dynamic structural data.

A detailed structural interpretation of our finding does not appear to be feasible on the basis of our current molecular understanding of protein stability. Molecular dynamics simulations, currently the only method that can address all components of the molecular partition function of a protein individually for all states, are not yet able to give reliable quantitative estimates of their relative contributions. However, it has become clear over the past two decades that, despite the high packing densities of proteins, residual conformational entropy in the folded state can by no means be neglected and may even surpass the entropy change upon folding (*47*). More recent simulations indicate that previously unexpected entropic terms can significantly contribute to the delicate free energy balance of protein stability. Vibrational flexibility, for instance, can increase upon secondary structure formation (*48*), especially in the case of β-structure (*49*). The only currently available experimental methods with the potential capability of addressing some of these issues are nuclear spin relaxation rate measurements (*50*, *51*; for a review, see ref *52*). In a recent study, Stone and co-workers (*53*) found a striking correlation between the stability and backbone flexibility of several protein G B1 domain mutants, suggesting that increased backbone conformational entropy is a means of protein stabilization. Similar analyses might be able to clarify whether related mechanisms are utilized to achieve the remarkable stability of proteins from thermophilic organisms.

ACKNOWLEDGMENT

We thank G. Hummer, T. Kiefhaber, and T. Oas for discussion, F. X. Schmid, D. Perl, and W. A. Eaton for access

to their stopped-flow spectrometers, and F. X. Schmid for helpful comments on the manuscript.

REFERENCES

1. Jaenicke, R., and Böhm, G. (1998) The stability of proteins in extreme environments, *Curr. Opin. Struct. Biol. 8*, 738−748.
2. Szilágyi, A., and Závodszky, P. (2000) Structural differences between mesophilic, moderately thermophilic and extremely thermophilic protein subunits: results of a comprehensive survey, *Struct. Folding Des. 8*, 493−504.
3. Sterner, R., and Liebl, W. (2001) Thermophilic adaptation of proteins, *Crit. Rev. Biochem. Mol. Biol. 36*, 39−106.
4. Makhatadze, G. I., and Privalov, P. L. (1995) Energetics of protein structure, *Adv. Protein Chem. 47*, 307−425.
5. Perl, D., Welker, C., Schindler, T., Schroder, K., Marahiel, M. A., Jaenicke, R., and Schmid, F. X. (1998) Conservation of rapid two-state folding in mesophilic, thermophilic and hyperthermophilic cold shock proteins, *Nat. Struct. Biol. 5*, 229−235.
6. Perl, D., and Schmid, F. X. (2002) Some like it hot: The molecular determinants of protein thermostability, *ChemBioChem 3*, 39−44.
7. Kawamura, S., Abe, Y., Ueda, T., Masumoto, K., Imoto, T., Yamasaki, N., and Kimura, M. (1998) Investigation of the structural basis for thermostability of DNA-binding protein HU from *Bacillus stearothermophilus*, *J. Biol. Chem. 273*, 19982−19987.
8. Welker, C., Böhm, G., Schurig, H., and Jaenicke, R. (1999) Cloning, overexpression, purification, and physicochemical characterization of a cold shock protein homolog from the hyperthermophilic bacterium *Thermotoga maritima*, *Protein Sci. 8*, 394−403.
9. Kremer, W., Schuler, B., Harrieder, S., Geyer, M., Gronwald, W., Welker, C., Jaenicke, R., and Kalbitzer, H. R. (2001) Solution NMR structure of the cold-shock protein from the hyperthermophilic bacterium *Thermotoga maritima*, *Eur. J. Biochem. 268*, 2527−2539.
10. Huang, G. S., and Oas, T. G. (1995) Submillisecond folding of monomeric lambda repressor, *Proc. Natl. Acad. Sci. U.S.A. 92* (15), 6878−6882.
11. Burton, R. E., Huang, G. S., Daugherty, M. A., Fullbright, P. W., and Oas, T. G. (1996) Microsecond protein folding through a compact transition state, *J. Mol. Biol. 263*, 311−322.
12. Burton, R. E., Huang, G. S., Daugherty, M. A., Calderone, T. L., and Oas, T. G. (1997) The energy landscape of a fast-folding protein mapped by Ala → Gly substitutions, *Nat. Struct. Biol. 4*, 305−310.
13. Kuhlman, B., Boice, J. A., Fairman, R., and Raleigh, D. P. (1998) Structure and stability of the N-terminal domain of the ribosomal protein L9: evidence for rapid two-state folding, *Biochemistry 37*, 1025−1032.
14. Kuhlman, B., Luisi, D. L., Evans, P. A., and Raleigh, D. P. (1998) Global analysis of the effects of temperature and denaturant on the folding and unfolding kinetics of the N-terminal domain of the protein L9, *J. Mol. Biol. 284*, 1661−1670.
15. Spector, S., and Raleigh, D. P. (1999) Submillisecond folding of the peripheral subunit-binding domain, *J. Mol. Biol. 293*, 763−768.
16. Sykes, B. D., and Hull, W. E. (1978) Fluorine nuclear magnetic resonance studies of proteins, *Methods Enzymol. 49*, 270−295.
17. Danielson, M. A., and Falke, J. J. (1996) Use of ^{19}F NMR to probe protein structure and conformational changes, *Annu. Rev. Biophys. Biomol. Struct. 25*, 163−195.
18. Gerig, J. T. (1989) Fluorine nuclear magnetic resonance of fluorinated ligands, *Methods Enzymol. 177*, 3−23.
19. Gerig, J. T. (1997) Fluorine NMR, in *On-Line Biophysics Textbook* (Bloomfield, V., Ed.) Biophysical Society, Bethesda MD (http://www.biophysics.org/btol).
20. Kim, H. W., Perez, J. A., Ferguson, S. J., and Campbell, I. D. (1990) The specific incorporation of labeled aromatic amino acids into proteins through growth of bacteria in the presence of glyphosate. Application to fluorotryptophan labeling to the H(+)-ATPase of *Escherichia coli* and NMR studies, *FEBS Lett. 272*, 34−36.
21. Roisch, U., and Lingens, F. (1980) The mechanism of action of the herbicide N-(phosphonomethyl)glycine: its effect on the growth and the enzymes of aromatic amino acid biosynthesis in *Escherichia coli*, *Hoppe-Seyler's Z. Physiol. Chem. 361*, 1049−1058.
22. Schindler, T., and Schmid, F. X. (1996) Thermodynamic properties of an extremely rapid protein folding reaction, *Biochemistry 35*, 16833−16842.
23. Pace, C. N. (1986) Determination and analysis of urea and guanidine hydrochloride denaturation curves, *Methods Enzymol. 131*, 266−280.
24. Gill, S. C., and von Hippel, P. H. (1989) Calculation of protein extinction coefficients from amino acid sequence data, *Anal. Biochem. 182*, 319−326.
25. Pace, C. N., Vajdos, F., Fee, L., Grimsley, G., and Gray, T. (1995) How to measure and predict the molar absorption coefficient of a protein, *Protein Sci. 4*, 2411−2423.
26. Budisa, N., Steipe, B., Demange, P., Eckerskorn, C., Kellermann, J., and Huber, R. (1995) High-level biosynthetic substitution of methionine in proteins by its analogs 2-aminohexanoic acid, selenomethionine, telluromethionine and ethionine in *Escherichia coli*, *Eur. J. Biochem. 230*, 788−796.
27. Bronskill, P. M., and Wong, J. T.-F. (1988) Suppression of fluorescence of tryptophan residues in proteins by replacement with 4-fluorotryptophan, *Biochem. J. 249*, 305−308.
28. Edelhoch, H. (1967) Spectroscopic determination of tryptophan and tyrosine in proteins, *Biochemistry 6*, 1948−1954.
29. Santoro, M. M., and Bolen, D. W. (1988) Unfolding free energy changes determined by the linear extrapolation method. 1. Unfolding of phenylmethanesulfonyl α-chymotrypsin using different denaturants, *Biochemistry 27*, 8063−8068.
30. Maurer, T., and Kalbitzer, H. R. (1996) Indirect referencing of ^{31}P and ^{19}F NMR spectra, *J. Magn. Reson., Ser. B 113*, 177−178.
31. van Geet, A. L. (1968) Calibration of the methanol and glycol nuclear magnetic resonance thermometers with a static thermistor probe, *Anal. Chem. 40*, 2227−2229.
32. Volkin, D. B., Mach, H., and Middaugh, C. R. (1995) Degradative covalent reactions important to protein stability, *Methods Mol. Biol. 40*, 35−63.
33. Sandström, J. (1982) *Dynamic NMR Spectroscopy*, Academic Press, New York.
34. Tanford, C. (1968) Protein denaturation, *Adv. Protein Chem. 23*, 218−282.
35. Fersht, A. R. (1999) *Structure and mechanism in protein science: a guide to enzyme catalysis and protein folding*, Freeman, New York.
36. Eaton, W. A., Munoz, V., Hagen, S. J., Jas, G. S., Lapidus, L. J., Henry, E. R., and Hofrichter, J. (2000) Fast kinetics and mechanisms in protein folding, *Annu. Rev. Biophys. Biomol. Struct. 29*, 327−359.
37. Privalov, P. L. (1979) Stability of proteins: small globular proteins, *Adv. Protein Chem. 33*, 167−241.
38. Wassenberg, D., Welker, C., and Jaenicke, R. (1999) Thermodynamics of the unfolding of the cold-shock protein from *Thermotoga maritima*, *J. Mol. Biol. 289*, 187−193.
39. Mücke, M., and Schmid, F. X. (1994) A kinetic method to evaluate the two-state character of solvent-induced protein denaturation, *Biochemistry 33*, 12930−12935.
40. Baxter, N. J., and Williamson, M. P. (1997) Temperature dependence of ^{1}H chemical shifts in proteins, *J. Biomol. NMR 9*, 359−369.
41. Arcus, V. L., Vuilleumier, S., Freund, S. M., Bycroft, M., and Fersht, A. R. (1995) A comparison of the pH, urea, and temperature-denatured states of barnase by heteronuclear NMR: implications for the initiation of protein folding, *J. Mol. Biol. 254*, 305−321.
42. Shortle, D. (1996) The denatured state (the other half of the folding equation) and its role in protein stability, *FASEB J. 10*, 27−34.
43. Smith, L. J., Fiebig, K. M., Schwalbe, H., and Dobson, C. M. (1996) The concept of a random coil. Residual structure in peptides and denatured proteins, *Folding Des. 1*, R95−R106.
44. Myers, J. K., Pace, C. N., and Scholtz, J. M. (1995) Denaturant *m* values and heat capacity changes: relation to changes in accessible surface areas of protein unfolding, *Protein Sci. 4*, 2138−2148.

45. Pohl, F. M. (1976) Temperature-dependence of the kinetics of folding of chymotrypsinogen A, *FEBS Lett. 65*, 293−296.
46. Oliveberg, M., Tan, Y. J., and Fersht, A. R. (1995) Negative activation enthalpies in the kinetics of protein folding, *Proc. Natl. Acad. Sci. U.S.A. 92*, 8926−8929.
47. Karplus, M., Ichiye, T., and Pettitt, B. M. (1987) Configurational entropy of native proteins, *Biophys. J. 52*, 1083−1085.
48. Ma, B., Tsai, C. J., and Nussinov, R. (2000) A systematic study of the vibrational free energies of polypeptides in folded and random states, *Biophys. J. 79*, 2739−2753.
49. Ma, B., and Nussinov, R. (1999) Explicit and implicit water simulations of a β-hairpin peptide, *Proteins 37*, 73−87.
50. Li, Z., Raychaudhuri, S., and Wand, A. J. (1996) Insights into the local residual entropy of proteins provided by NMR relaxation, *Protein Sci. 5*, 2647−2650.
51. Yang, D., and Kay, L. E. (1996) Contributions to conformational entropy arising from bond vector fluctuations measured from NMR-derived order parameters: application to protein folding, *J. Mol. Biol. 263*, 369−382.
52. Ishima, R., and Torchia, D. A. (2000) Protein dynamics from NMR, *Nat. Struct. Biol. 7*, 740−743.
53. Stone, M. J., Gupta, S., Snyder, N., and Regan, L. (2001) Comparison of Protein Backbone Entropy and β-Sheet Stability: NMR-Derived Dynamics of Protein G B1 Domain Mutants, *J. Am. Chem. Soc. 123*, 185−186.
54. Koradi, R., Billeter, M., and Wüthrich, K. (1996) MOLMOL: a program for display and analysis of macromolecular structures, *J. Mol. Graphics 14*, 29−32.

BI026293L